Continuous dynamic recrystallization during hot torsion of an aluminum alloy.

IOP Conf. Series: Journal of Physics: Conf. Series **1270** (2019) 012049 doi:10.1088/1742-6596/1270/1/012049

Continuous dynamic recrystallization during hot torsion of an aluminum alloy.

M C Poletti[1], T Simonet-Fotso[1], D Halici[2], D Canelo-Yubero[1], F Montheillet[3], D Piot[3], Z Kovács[4], N Schell[5], D Tolnai[5]

1Institute of Materials Science Joining and Forming, Graz University of Technology, Graz, Austria;
2Andritz AG, Graz, Austria
3 Physique et Mécanique des Matériaux, Ecole des Mines Saint Etienne, Saint Etienne, France
4 Department of Materials Physics, Lorand Eötvös University. Budapest, Hungary
5. Institute of Materials Research, Helmholtz Zentrum Geesthacht, Geesthacht, Germany
e-mail address corresponding author: cecilia.poletti@tugraz.at

Abstract. Most commercial aluminum alloys are characterized by dynamic recrystallization at very large deformations in a continuous manner. The present study deals with the characterization and modeling of the evolution of the microstructure of an aluminum wrought alloy at large plastic deformations. Hot torsion tests of the AA6082 aluminum alloy are carried out using the thermomechanical simulator Gleeble®3800 in a wide range of temperatures and strain rates. The use of water quenching immediately after deformation avoids any static restoration during cooling. Microstructural investigations are carried out by means of electron back scattered diffraction using a scanning electron microscope to determine the grain and subgrain structures, as well as the misorientation distributions. In-situ synchrotron radiation tests during hot torsion are used to confirm the continuous dynamic recrystallization (CDRX) by the evidence of the conversion of low angle boundaries (LAGBs) into high-angle boundaries (HAGBs) and the formation of new texture. Experimental investigations show that CDRX starts with the formation of LAGBs at low strains (center of the sample). By subsequent straining (close to the surface of the sample), the accumulation of dislocations at the LAGBs causes an increase in their misorientation until a critical value is reached and LAGBs transforms into HAGBs. The developed model consists of a microstructural model, equation rates and constitutive equations. The microstructure is described by three internal variables. Their rates are evaluated using the Kocks-Mecking model. The modelled and experimental flow stresses show softening due to the consumption of dislocations and the continuous formation of new HAGBs.

1. Introduction

Dynamic recrystallization (DRX) often occurs when metallic parts undergo hot deformation. Discontinuous dynamic recrystallization (DDRX) is a well-known process that occurs in moderate and low stacking fault energy (SFE) materials by nucleation followed by grain growth [1,2]. When dealing with high SFE metals two different mechanisms have been proposed in the literature to explain the modification of the microstructure: 1) continuous dynamic recrystallization (CDRX) correlated with a change in texture [1-3], and 2) geometric dynamic recrystallization (GDRX) where texture remains unaltered [4,5]. The CDRX implies a smooth change in the microstructure by a progressive formation and rotation of subgrains as deformation proceeds. Thus, the amount of dislocations forming the walls of the subgrains increases, resulting in a total misorientation increment. During this process, subgrain

boundaries or low angle grain boundaries (LAGB) are converted into high angle grain boundaries (HAGB) [3]. On the other hand, the GDRX is consistent with Taylor theory requirements [6] and involves formation of subgrains followed by migration and pinching off of original HAGBs [7]. Although the models are based on different mechanisms to explain the microstructure evolution, both mechanisms can take place simultaneously [8]. Finally, it still has to be clarified if the formed HAGBs are a consequence of the transformation from LAGB or by HAGB migration. [9,10].

This work aims at elucidating and modelling the physical processes occurring during plastic deformation up to large strains of a high SFE aluminum alloy. The evolution of the microstructure could be tracked using in-situ high energy synchrotron radiation diffraction (HEXRD) during a torsion test.

2. Experimental methods

Aluminum samples were hot deformed at very large strains by using torsion tests. The microstructure was characterized at the center and close outer surface of the torsion sample after deformation and water quenching. The alloy used in this study is an AA6082 (AlSi1MgMn) aluminum alloy produced by the company Zultner Metall GmbH by hot extrusion and aged to T6 condition. Torsion samples were prepared with a gauge length of 20 mm and a gauge diameter of 10 mm.

Hot torsion tests using a Gleeble ® 3800 were carried out to produce deformed samples and flow curves. Temperature control during deformation was done with a thermocouple welded at the fixed border of the gauge. The tests were carried out between 350 and 500°C, with effective strain rates of 0.01-1 s^{-1}. Equivalent flow stresses and strains were calculated from the torque and revolution data, respectively. All samples were water quenched after deformation to avoid any further restoration.

The microstructure of the deformed samples was observed across their gauge to obtain information with respect to the strain, this last varying from zero in the middle axe along the gauge to a maximum value at outer surface. Scanning electron microscopy (SEM) was conducted using a Tescan Mira3 SEM equipped with a Hikari Electron Backscattered Diffraction (EBSD) camera to characterize grain sizes, local misorientations given by Kernel Average Misorientation (KAM) and misorientation distributions.

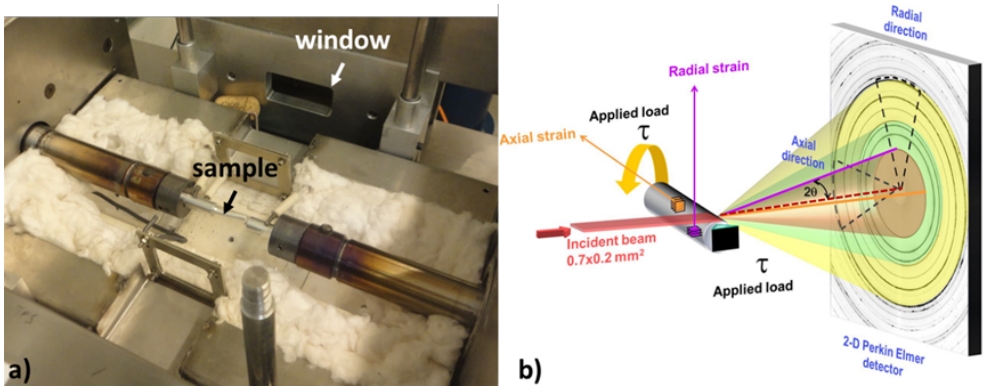

Figure 1 In-situ torsion test configuration a) furnace with a window transparent to X-rays, and b) drawing of the set up with incident beam close to surface of sample

X-Ray diffraction measurements using synchrotron radiation were done in a thin slice of material close to the outer surface while torsion was applied on the Al alloy at high temperatures (see Figure 1). The collected Debye-Scherrer rings were processed to produce the azimuthal angle (Ψ) - effective strain (AS) plots, showed together with the τ_{eff} - ε_{eff} curves in Figure 6.

3. Modelling

The model developed based on [11] consists of three main components: 1) internal variables that constitute the microstructure, 2) evolution of these internal variables, and 3) constitutive equations.

The microstructure was described as an aggregate of subgrains delimited by LAGBs and HAGBs. Three internal variables were used: the density of dislocations inside the subgrains (ρ_i), the average

subgrain size (D), and the fraction of LAGBs (f_{LAGB}). During a strain increment dε dislocation density increases by $hd\varepsilon$ and $r\rho_i d\varepsilon$ annihilate or are incorporated in LAGBs by dynamic recovery. A part $\rho_i dV$ is consumed by the migration of HAGBs.

$$d\rho_i = hd\varepsilon - r\rho_i d\varepsilon - \rho_i S_V f_{HAGB} v_M d\varepsilon/\dot{\varepsilon} \quad (1)$$

f_{HAGB} = fraction of HAGBs, v_M = average velocity of grain boundaries, S_V is the surface of boundaries, and h and r are the hardening and recovery coefficients, respectively. Among the recovery part, a fraction β is annihilated, a fraction $(1-\beta)\alpha$ is consumed by the formation of new LAGB, and the rest $(1-\beta)(1-\alpha)$ is absorbed by the existent LAGBs and HAGBs. The incorporation of dislocations in LAGBs induces a misorientation increase ($d\theta$):

$$d\theta = (1-\beta)(1-\alpha)\frac{b}{2n}D(r\rho_i)d\varepsilon \quad (2)$$

n = constant, b is the Burger's vector, . The evolution in total area of boundary per unit volume is given by $dSV = dSV^{+} - dSV^{-}$, where dSV^{+} corresponds to the area of LAGBs created during straining and dSV^{-} corresponds to the area of boundary eliminated by the HAGBs migration:

$$dS_v{}^{+} = (1-\beta)\alpha\frac{b}{n\theta_0}(r\rho_i)d\varepsilon \text{ and } dS_v{}^{-} = S_V dV = \frac{S_V{}^2 f_{HAGB} v_M d\varepsilon}{\dot{\varepsilon}} \quad (3)$$

The fraction of LAGBs and the density of dislocations forming the LAGBs, ρ_w were calculated using the distribution function of the misorientations ($\varphi(\theta)$).

$$f_{LAGB} = \int_{\theta_0}^{\theta_c}\varphi(\bar{\theta},\varepsilon)d\theta \quad \text{and} \quad \rho_w = \left(\frac{2.n}{b.D}\right)\int_{\theta_0}^{\theta_c}\varphi(\bar{\theta},\varepsilon).\bar{\theta}d\theta \quad (4)$$

θ_0 = minimum misorientation angle of new created LAGB, $\bar{\theta}$ = mean misorientation, and θ_c = critical angle for the transformation of LAGB into HAGB. The flow stresses (Figure 2) were calculated using the Taylor factor M, the shear modulus G, and material constants α_1, A_1 and A_2.

$$\sigma = M\alpha_1 Gb\left(A_1\sqrt{\rho_i} + A_2\sqrt{\rho_w}\right) \quad (5)$$

4. Results and discussions

The experimental and calculated flow stresses are plotted in Figure 2 for different deformation conditions. The model could capture the temperature and strain rate influences on the stress. Furthermore, flow softening is observed and calculated for all the conditions.

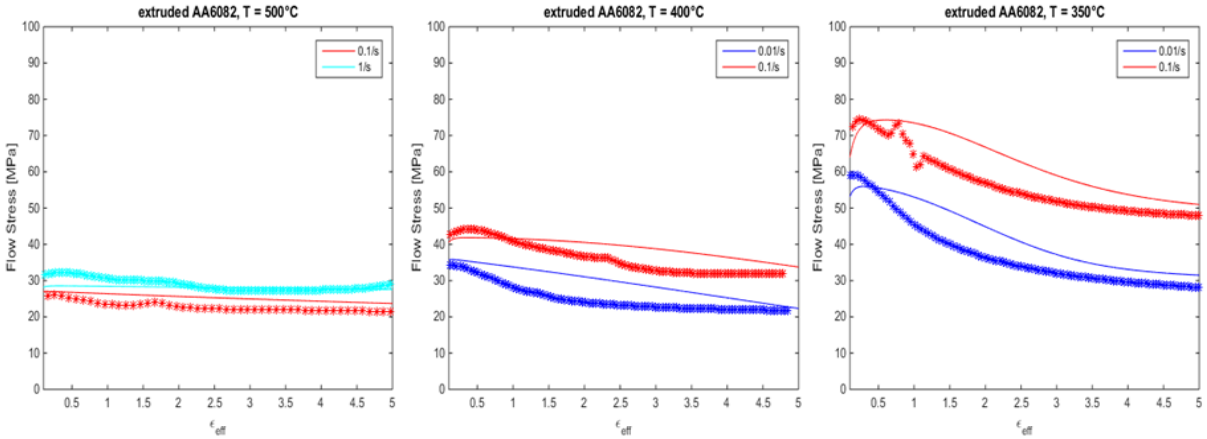

Figure 2. Experimental (symbols) and modelled (full line) flow stresses at different conditions

The effect of the strain on the microstructure can be followed from close to the centre (low strain) across the diameter to the edge of the sample (large strains) in Figure 3a) and Figure 3b) and c), respectively. By increasing the deformation, a continuous formation of new HAGB and grain refinement was observed in general. Furthermore, the recrystallized grain size as well as the grade of recrystallization for a given strain is shown to be dependent on the temperature and strain rate. In agreement, the flow steady state is achieved at large strains. The steady state is achieved faster the lower the strain rate and the higher the temperature are.

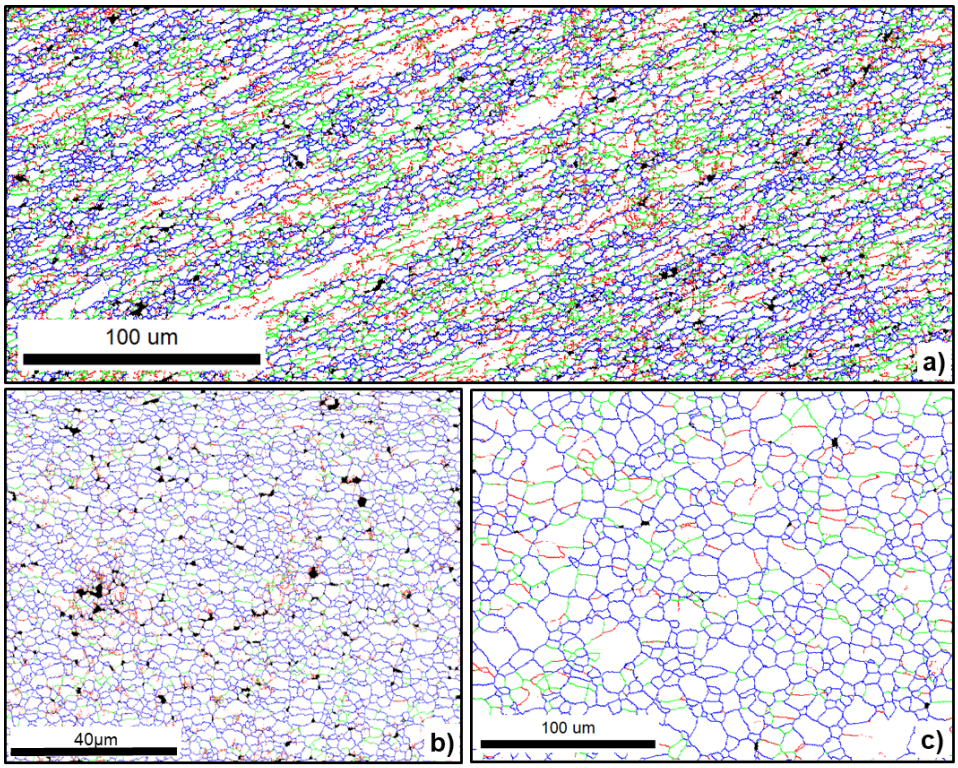

Figure 3. Map of boundaries: red between 2-5°, green between 5-11° and blue above 11°. Samples deformed at 0.1s^{-1} and a) 350°C, b) 350°C and c) 500°C. Pictures b) and c) are obtained from samples taken from the edge (strains close to 5), and picture a) shows less HAGB in the middle of the sample. Note the differences in the scales.

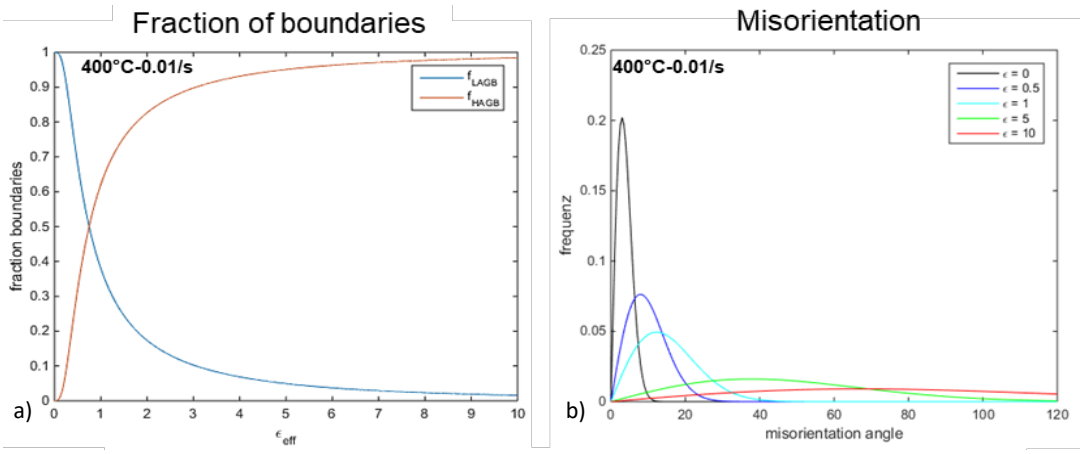

Figure 4. Microstructural outputs of the model: a) f_{HAGB} and f_{LAGB} with increasing strain, and b) evolution of the misorientation distributions with the strain.

The starting microstructure is modelled as being formed by one coarse grain. Therefore, LAGBs are firstly formed and then consumed during recovery and CDRX (Figure 4a). Furthermore, the evolution of the misorientation refers to what is formed during the deformation (Figure 4b), and it does not account for the HAGBs existing prior to deformation. The distributions of measured misorientations are shown for different conditions in Figure 5. LAGBs fraction decrease by increasing both, the strain and the strain rate. The distributions show large values of misorientations for the original grains, and very low values for the formation of LAGBs. The increasing values in the 15-40° range might correspond to the ones formed during CDRX, in agreement with the predictions of the model shown in Figure 4b).

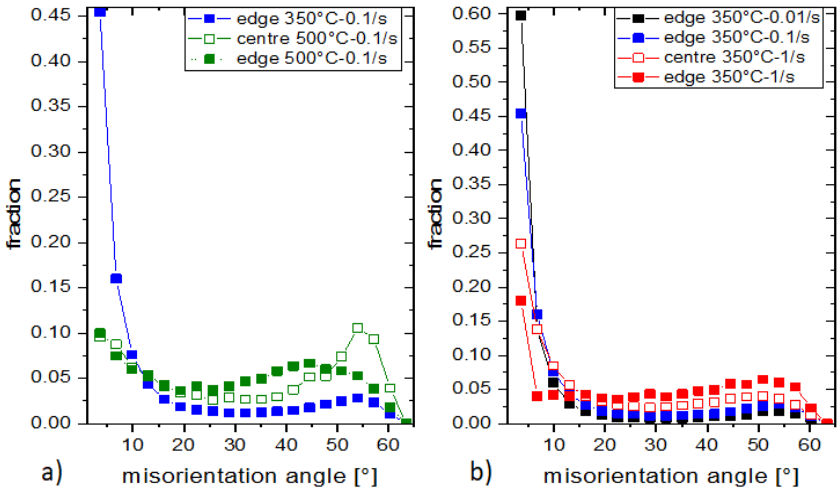

Figure 5. Misorientation angle distributions showing the influence of a) temperature and strain b) strain rate and strain.

The analysis of the in-situ data during hot torsion is shown in Figure 6 (AS-plots). It indicates a strong (111) starting texture and a less intense (200)-fibre texture due to the extrusion process of the initial condition. During the early stages of deformation, the high intensity regions broaden monotonically due to the formation of a substructure up to an effective strain of ε_{eff}~ 0.7. The resulting final texture is different from the starting one, being a strong proof of the CDRX process.

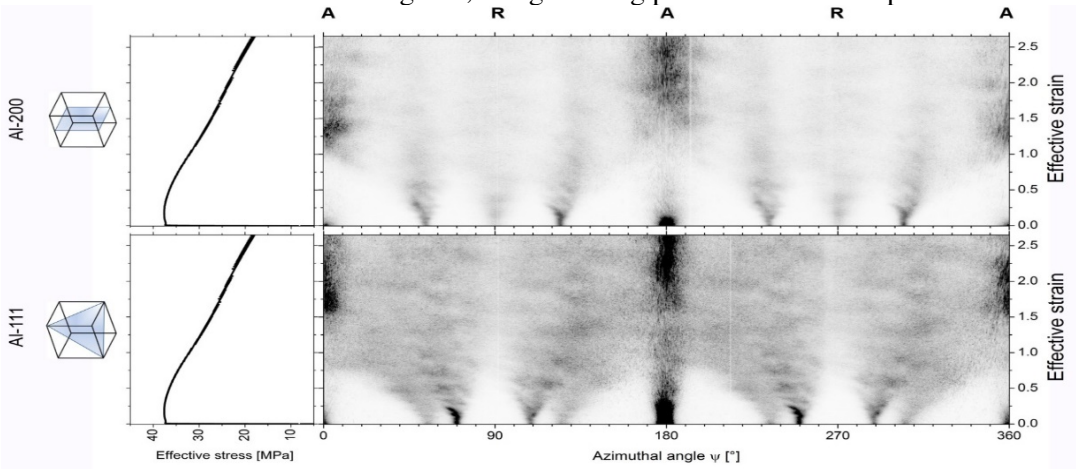

Figure 6. AS-plots for the Al-200 and Al-111 crystallographic planes.

Finally, the grain size was calculated as being decreased with the strain (**Figure 7**a). The driving force for CDRX is given by the pressure at the LAGBs as a result of the dislocation density, meaning that low temperatures and high strain rates are favorable. On the other hand, the mobility of the boundary

increases exponentially with the temperature, therefore accelerating the CDRX and decreasing at the same time the driving force by the rapid consumption of dislocations. Measured grain sizes (Figure 7b) show in general larger values than the modelled ones.

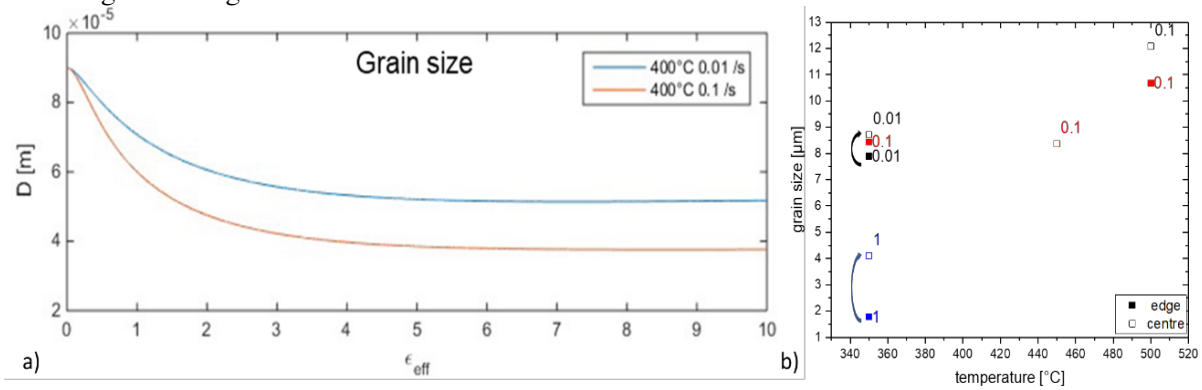

Figure 7. a) Calculated evolution of the grain size b) measured grain size at different temperatures, strains and strain rates (blue for $1s^{-1}$, red for $0.1s^{-1}$, and black for $0.01s^{-1}$).

5. Summary and conclusions

We could prove, quantify and model the microstructural and stress evolution of AA6082 aluminum alloy during large deformations at high temperatures. We found that the grain refinement and the decrement of dislocation densities within grains (KAM) can be described by CDRX. We described the continuous dynamic recrystallization as follows: during deformation at high temperatures, cell formation happens (wall dislocation density increases rapidly) by dynamic recovery. As the deformation increases, the wall dislocation density reaches a maximum value, then decreases due to the formation of new HAGBs. The softening is due to the absorption of dislocation by the existent and also the newly created boundaries.

6. Acknowledgments

The authors would like to thank to Ricardo Buzolin for the EBSD measurements. The work was supported by the Austrian Science Fund (FWF) within the stand alone project P 27471.

References

[1] Humphreys F J, Hatherly M 2004 *Recrystallization and related annealing phenomena* (Elsevier, Oxford).
[2] Sakai T, Belyakov A, Kaibyshev R, Miura H and Jonas J J 2014 *Prog. Mater. Sci.* **60** 130
[3] Gourdet S and Montheillet F 2000 *Mater. Sci. Eng. A* **283** 274
[4] McQueen H J, Knustand O, Ryum N, Solberg J K 1985 *Scripta Metall. Mater.* **19** 73
[5] Solberg J K, McQueen H J, Ryum N and Nes E 1989 *Part I, Philos. Mag. A* **60** 447
[6] McQueen H J, Kassner M E 2004 *Scripta Mater.* **51** 461
[7] Gholinia A, Pragnell P B and Markushev M V 2000 *Acta. Mater.* **48** 1115
[8] Pari Jr. L D and Misiolek V D 2008 *Acta Mater.* **56** 6174
[9] Driver J 2018 *Matter. Lett.* **222** 135
[10] Huang K and Logé R E 2016 *Mater. Design.* **111** 548
[11] Gourdet S, Montheillet F 2003 *Acta Mater.* **51-9** 2685